Hydrogen-induced atomic structure evolution of the oxygen-chemisorbed Cu(110) surface

Weitao Shan, Qianqian Liu, Jonathan Li, Na Cai, Wissam A. Saidi, and Guangwen Zhou

Citation: J. Chem. Phys. **145**, 234704 (2016); doi: 10.1063/1.4972070
View online: http://dx.doi.org/10.1063/1.4972070
View Table of Contents: http://aip.scitation.org/toc/jcp/145/23
Published by the American Institute of Physics

Hydrogen-induced atomic structure evolution of the oxygen-chemisorbed Cu(110) surface

Weitao Shan,[1] Qianqian Liu,[1] Jonathan Li,[2] Na Cai,[1] Wissam A. Saidi,[3] and Guangwen Zhou[1,a)]

[1]*Department of Mechanical Engineering and Materials Science and Engineering Program, State University of New York, Binghamton, New York 13902, USA*

[2]*Department of Physics, Applied Physics and Astronomy and Materials Science and Engineering Program, State University of New York, Binghamton, New York 13902, USA*

[3]*Department of Mechanical Engineering and Materials Science, University of Pittsburgh, Pittsburgh, Pennsylvania 15261, USA*

(Received 5 July 2016; accepted 29 November 2016; published online 20 December 2016)

Using a combination of scanning tunneling microscopy (STM) and density functional theory (DFT) modeling, we determine the mechanism of the atomic structural evolution of the oxygenated Cu(110) surface induced by the reaction of adsorbed hydrogen with chemisorbed oxygen in the Cu(110)-$c(6 \times 2)$-O structure. Our STM observations show that the reconstructed Cu(110)-$c(6 \times 2)$-O surface undergoes a phase transition to the (2×1)-O reconstruction in the course of oxygen loss induced by the reaction with H_2 gas. Using DFT modeling, we find that the surface phase transition is initiated via the adsorption of molecular hydrogen on the chemisorbed oxygen, which results in the formation of H_2O molecules that desorb spontaneously from the surface. The loss of chemisorbed oxygen induces the $c(6 \times 2) \rightarrow (2 \times 1)$ transition that involves the diffusion of Cu—O—Cu chains along the $\langle \bar{1}10 \rangle$ direction. *Published by AIP Publishing.* [http://dx.doi.org/10.1063/1.4972070]

I. INTRODUCTION

Transition metals such as Cu are now widely used catalysts in catalytic oxidation processes to produce petroleum-based compounds.[1] During the oxidation process, molecular oxygen dissociates over the metal surface to form chemisorbed oxygen. Meanwhile, hydrogen can be produced at the metal surface during the catalytic reaction, either directly through the dissociation of water molecules or disproportionation of hydroxyl groups. Therefore, a fundamental understanding of the interaction of hydrogen with chemisorbed oxygen on metal surfaces is relevant to various technologically important processes such as the water-gas-shift reaction, methanol synthesis and oxidation, for which Cu-based catalysts are well-known to be active and both oxygen and hydrogen are involved either as reactants or reaction products present on the metal surface.

There have been extensive studies on the interaction of hydrogen with metallic surfaces. Experimentally, it was shown by Österlund *et al.* that the Cu(110) surface reconstructs into a "missing-row" structure upon exposure to H_2 gas.[2] The H_2 adsorption on the Ni(110) surface was also shown to reconstruct the surface.[3] The H-chemisorption induced surface reconstructions on other transition metals, such as Pt and Ir, were also reported by Ibbotson *et al.*[4] and Engstrom *et al.*[5] Density functional theory (DFT) study by Hammer *et al.* provided an atomic understanding of the H_2 dissociative adsorption on the Cu(111) surface.[6] Mattsson *et al.*[7] and Kresse *et al.*[8,9] also applied DFT to gain a better insight of the H adsorption on Ni. In general, dissociative adsorption of H_2 on the metal surfaces leads to a surface reconstruction and finally to the formation of a hydride compound.[10] Nonetheless, the study on the interaction of hydrogen with chemisorbed oxygen on metal surfaces is still very limited. It is well known that metal surfaces develop well-defined reconstructions upon oxygen chemisorption. However, in many cases, it is still not well understood how the atomic structure of the oxygenated metal surfaces evolves upon reacting with hydrogen.

The focus of the present work is therefore to understand the evolution of the atomic structure of the oxygenated Cu surface upon its exposure to H_2 gas and elucidate the microscopic process underlying such structure evolution. Cu has been studied as a prototype system dealing with oxygen surface chemisorption. Particularly, oxygen chemisorption on Cu(110), the most open of the low-index surfaces, is among the most studied systems. Upon exposure to oxygen gas, Cu(110) undergoes a sequential pathway of surface reconstructions.[11–18] It first reconstructs to the added-row (2×1)-O structure with a saturated oxygen coverage of 0.5 monolayer (ML), which is characterized by the formation of Cu—O—Cu chains along the [001] direction in every other $[1\bar{1}0]$-(1×1) spacing of the substrate. Upon further exposure to oxygen gas, the (2×1)-O phase transitions to the $c(6 \times 2)$-O reconstruction with a saturated oxygen coverage of 2/3 ML, which contains two adjacent Cu—O—Cu chains growing along the [001] direction in every three $[1\bar{1}0]$-(1×1) spacings of the Cu(110) substrate.[11,19] Previously, numerous efforts have been devoted to studying this phase transition on the Cu surface. Jensen *et al.* conducted scanning tunneling microscopy (STM) investigations on the dynamics of the chemisorbed-oxygen-induced surface reconstruction on the Cu(110) surface.[20,21] The experimental work presented by Kern *et al.* showed that the

a)Author to whom correspondence should be addressed. Electronic mail: gzhou@binghamton.edu

added Cu—O—Cu rows self-assemble into two-dimensional islands.[22] Frechard and Van Santen used DFT calculations to study atomic O adsorption on the Cu(110) surface and found that the (2 × 1) added-row reconstruction can lower the system energy.[23] Theoretical studies by Liem *et al.* elucidated the growth pathway of the (2 × 1) added-row reconstruction and the dissociation pathway of O_2 molecules on the Cu(110) surface.[24,25] Using DFT modeling, Duan *et al.*[26] investigated the relation between the O surface coverage and the stable structure and constructed a surface phase diagram for both Cu(100) and (110). Zhou *et al.* further showed that the presence of surface steps can promote the formation of the bulk-like oxide (i.e., Cu_2O) without involving the restructuring of the Cu surface.[27] The wealth information from the O/Cu(110) system makes it an ideal system to elucidate how hydrogen adsorption induces the surface structure evolution, which not only implies a morphological change but may also lead to remarkable changes in chemical reactivity. For example, it was shown that methanol oxidation is very sensitive to oxygen-chemisorption-induced reconstructions on Cu surfaces, and the surface coverage of adsorbed O atoms can enhance the catalytic ability of the Cu catalyst.[28–33] However, even though Cu-based catalysts have been widely used for catalytic oxidation processes, the hydrogen-induced reactions on oxygen-chemisorbed Cu catalyst surfaces are not well studied. Identification of the surface structure formed from the dynamic interaction of hydrogen with chemisorbed oxygen is necessary to obtain the fundamental insight into the surface reactivity of the oxygen-metal systems.

II. EXPERIMENTAL AND COMPUTATIONAL METHODS

The experiments were performed with an ultrahigh vacuum (UHV) variable-temperature STM system (Omicron VT-STM XA) with a base pressure of ~1×10^{-11} Torr. Our experiments involved a two-step process. At first, an atomically clean Cu(110) surface was exposed to oxygen gas to form a well-reconstructed Cu(110)-$c(6 \times 2)$ surface structure, as shown in our previous study.[11,19] To study H_2 reaction with the chemisorbed oxygen, the Cu(110)-$c(6 \times 2)$ surface was then exposed to the flow of hydrogen gas at elevated temperatures. STM imaging was used to determine the atomic structure evolution induced by the H_2 exposure. The Cu(110) single crystal is a "top-hat" disk (1 mm thick and 8 mm in diameter), purchased from Princeton Scientific Corp., cut to within 0.1° to the (110) crystallographic orientation and polished to a mirror finish. The Cu(110) surface was prepared by repeated cycles of Ar^+ sputtering at room temperature (5×10^{-5} Torr of Ar^+, 1 μA cm^{-2}, 1.0 keV) followed by annealing at 600 °C for 10 min. Cleanliness of the Cu(110) surface was checked by several methods such as Auger electron spectroscopy (AES), X-ray photoelectron spectroscopy (XPS), and STM imaging. Especially, STM imaging is extremely sensitive to any local impurities. Due to the high mobility of surface atoms for a clean surface, step edges appear fuzzy in STM imaging. If there are any impurities, they tend to locally pin surface steps and the fuzzy feature disappears. In this way, the cleanliness of the surface can be checked locally by STM imaging prior to O_2 dosing at the pressure of 1×10^{-5} Torr and T = 350 °C to form a fully reconstructed Cu(110)-c(6 × 2)-O surface. The Cu(110)-$c(6 \times 2)$-O surface was then exposed to H_2 at the pressure varying from 1×10^{-8} Torr to 5×10^{-5} Torr and T = 150 °C. An electrochemically etched polycrystalline tungsten wire was used to make the STM tips, which were flashed at 1 kV and 2 mA for several times to evaporate adsorbates and native oxide before STM imaging. The O_2 dosing was performed in a separate chamber from the STM chamber to ensure the pristine nature of the tungsten tip. All the STM images were acquired at room temperature in constant-current mode with bias on the sample (e.g., Figs. 1 and 5).

In our experiment, gas dosing was performed in a sample preparation chamber (with a base pressure of 3×10^{-10} Torr), followed by sample transfer to the STM chamber (with a base

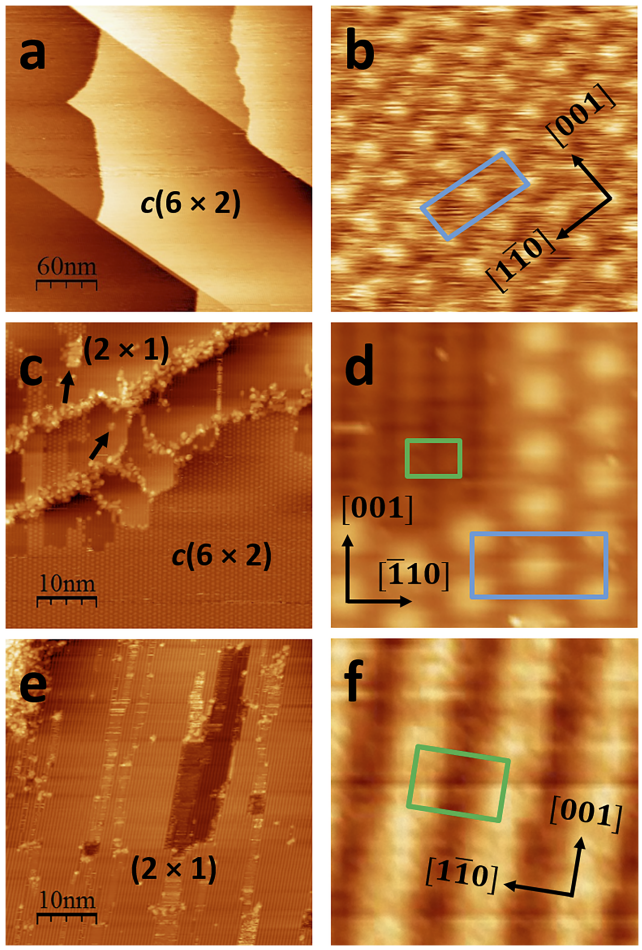

FIG. 1. Topographic STM images of Cu(110)-c(6 × 2) surface reconstruction process and the magnified atomic scale images. The c(6 × 2) and (2 × 1) configurations are, respectively, delineated by blue and green lines in the STM images. (a) STM image of the Cu(110) surface after the oxygen exposure at T = 350 °C and $pO_2 = 1 \times 10^{-5}$ Torr for 40 min; (b) atomically resolved STM image of (a), showing that the entire surface is covered by the c(6 × 2) reconstruction; (c) STM image of the Cu(110)-c(6 × 2) surface after H_2 exposure at 150 °C and the H_2 pressure of 1×10^{-8} Torr for 90 min and then $pH_2 = 1 \times 10^{-7}$ Torr for 2 h; (d) zoom-in STM of (c) showing the coexistence of c(6 × 2) and (2 × 1) domains; (e) STM image of the Cu(110)-c(6 × 2) surface after the additional H_2 exposure at T = 150 °C and $pH_2 = 5 \times 10^{-5}$ Torr for 15 h and 40 min; (f) zoom-in STM image of (e) showing that the entire surface is now covered with the (2 × 1) reconstruction. The tunneling conditions for the STM imaging are $I_T = 0.4$ nA and $V_B = -1$ V for (a) and (b), $I_T = 0.2$ nA and $V_B = -1$ V for (c) and (d), and $I_T = 0.5$ nA and $V_B = -1.5$ V for (e) and (f).

pressure of 1×10^{-11} Torr) for imaging the surface. Particular care was taken to minimize any potential contamination by baking the gas lines and then flushing the lines with H_2 gas for several times before dosing gases into the preparation chamber. A mass spectrometer was also used to monitor the gas composition in the preparation chamber. H_2 dosing was performed in an added-on manner, i.e., the sample was exposed to H_2 for ~30 min each time in the preparation chamber and then transferred to the STM chamber. While performing STM imaging, the preparation chamber was pumped down to a base pressure of 3×10^{-10} Torr for the subsequent H_2 dosing. In this way, any effect from hydrogen-wall reactions can be minimized.

Density functional theory[34–38] calculations were performed using the Vienna *ab initio* simulation package (VASP).[39–42] PW91 generalized gradient approximation (GGA)[43] and projector augmented wave (PAW)[44] potentials were adopted to carry out these calculations. Our computational framework is similar to our previous studies.[11,19,45–48] The cut-off energy was set to be 380 eV, which was verified to yield adsorption energy convergence to 1 meV after a comparative testing using a higher cut-off energy of 450 eV. All of our calculations were spin-averaged, which we have verified to be adequate as there was no significant difference when spin polarization is turned on. We used a $2 \times 4 \times 1$ Monkhorst-Pack-grid[49] in our calculations, which we have verified to be adequate by comparing to results obtained using a $4 \times 8 \times 1$ k-grid. We calculated the lattice constant of Cu to be 3.63 Å, which is in good agreement with previous calculations.[19,25,26] The surface was modeled by a periodically repeated five-layer $c(6 \times 2)$ slab with only the bottom two layers fixed. Atomic coordinates were allowed to move until the maximum force was less than 0.015 eV/Å. A vacuum spacing of 12 Å along the z-axis direction was used to separate the successive slabs as done in our previous study.[19] Further, we have also investigated whether van der Waals (vdW) interactions are important in our systems. We applied Tkatchenko-Scheffler (TS) dispersion correction,[50] which has been applied successfully to many systems.[51–54] Our results indicate that vdW interactions are minimal, and thus can be safely ignored from our study.

We investigated the adsorption of both atomic and molecular hydrogen in our DFT modeling and examined the surface structure evolution. For the H_2 molecule adsorption, we investigated configurations where the H_2 bond is vertical and parallel to the surface. The most stable configuration identified after an H/H_2 has been adsorbed is used as a starting configuration for loading the next H/H_2 to be adsorbed. The H/H_2 adsorption energy is computed using the equation

$$E_{ads} = E_{H/slab} - E_{slab} - \frac{n}{2}E_{H_2}, \quad (1)$$

where E_{ads} is the adsorption energy, $E_{H/slab}$ is the free energy of the slab with one H atom or one H_2 molecule, E_{slab} is the free energy of the slab without adsorbed hydrogen, E_{H_2} is the free energy of an isolated H_2 molecule, which was calculated using a cubic box with a side length of 17 Å, and n is the number of H atoms in the system (for H_2, $n = 2$). Only one H atom or H_2 molecule was added into the system at each time.

The reaction of hydrogen with chemisorbed oxygen results in the formation of H_2O molecules that desorb from the surface, which is accompanied with the concomitant restructuring of the surface involving the migration of Cu and O atoms left behind. For modeling the surface reconstruction process, the same slab was used to keep consistent with the hydrogen adsorption calculations. In our calculations, only the most unstable atom (Cu atom with the lowest vacancy formation energy or O atom with lowest adsorption energy) was removed from the cell each time. To gauge the propensity of an atom to be removed from the surface and its stability, we computed the vacancy formation energy defined as

$$E_f = E_{slab/vac} + E_{atom} - E_{slab}, \quad (2)$$

where E_f is the vacancy formation energy, $E_{slab/vac}$ is the free energy of the slab with one vacancy, E_{atom} is the free energy of one single atom in the pure substance, E_{slab} is the free energy of the slab without the vacancy. If the vacancy formation energy of the atom equals to or less than zero, this atom is unstable and tends to leave from the cell. Meanwhile, we also modeled the diffusion pathway and associated energy barriers by using the nudged elastic band (NEB) method,[55] where at least five intermediate images were added in between the initial and final states. The atomic structures were visualized using VESTA.[56]

III. RESULTS AND DISCUSSION

A. Experimental results

The clean Cu(110) surface was first exposed to the flow of oxygen gas to form the well-defined Cu(110)-$c(6 \times 2)$ reconstruction that contains two adjacent [001]-oriented Cu—O—Cu chains in every three $[1\bar{1}0]$-(1×1) lattice spacings.[11,19] Fig. 1(a) shows a representative STM image of typical large areas of the Cu(110)-$c(6 \times 2)$ surface formed by the oxygen exposure under the condition of $pO_2 = 1 \times 10^{-5}$ Torr and T = 350 °C for 40 min (exposure = 24 000 L). It can be seen that the surface consists of large, atomically flat terraces separated by straight and parallel atomic steps along with irregularly shaped steps in the oblique direction crossing the parallel ones. STM height profile analysis shows that most steps have a height of ~1.3 Å, consistent with the height of monoatomic steps on Cu(110). Fig. 1(b) is a typical high-resolution STM image revealing that the entire surface is fully covered by the $c(6 \times 2)$ reconstruction, where the unit cell is outlined in blue.

The Cu(110)-$c(6 \times 2)$ surface was then exposed to the flow of H_2 gas at 150 °C. Fig. 1(c) shows an STM image of the surface morphology after more than 3 h of the H_2 exposure. It can be seen that the surface underwent significant roughening after the H_2 exposure with the formation of nanoparticles aggregated mostly along step edges and some scattered on the terrace. Meanwhile, the upper and lower terraces exhibit domains of different structures. Fig. 1(d) is a zoom-in topographic STM image from Fig. 1(c), which shows the formation of parallel atomic chains that are bordered by the parent $c(6 \times 2)$ reconstructed region. Using the existing $c(6 \times 2)$ domain as reference, we can find that the newly formed chains are oriented along the bulk [100] direction of the substrate and the lateral spacing of these chains is 5 Å. These structure features show the row characteristic of the (2×1) restructuring, which is characterized by the formation of Cu—O—Cu chains growing preferentially along the [001] direction in every other

[1$\bar{1}$0]-(1 × 1) spacing (i.e., 5 Å) of the substrate. Compared to the $c(6 \times 2)$ structure that has a saturated oxygen coverage of θ = 2/3, the (2 × 1) reconstruction has a smaller saturated oxygen coverage θ = 1/2.[25,26,57] Because the original surface is fully covered by the $c(6 \times 2)$ reconstruction, the formation of the (2 × 1) regions is related to the loss of chemisorbed oxygen in the original $c(6 \times 2)$ structure, which is induced by the reaction of the chemisorbed oxygen with adsorbed hydrogen to form H_2O molecules that can easily desorb from the surface.

The bright protrusions in the $c(6 \times 2)$ region shown in Fig. 1(d) are Cu atoms bonding laterally (i.e., along the [1$\bar{1}$0] direction) with the O atoms within the adjacent [001]-oriented Cu—O—Cu chains that do not show up in the STM image. The protrusions in the $c(6 \times 2)$ region are higher than the Cu atoms within the Cu—O—Cu chains in the (2 × 1) region by 0.6 Å. This height difference is smaller than the monoatomic step height (1.3 Å) of Cu(110). Instead, it is consistent with the DFT calculations of the height difference between the (2 × 1) and $c(6 \times 2)$ domains formed on the same terrace, i.e., the $c(6 \times 2)$ reconstruction shows up as a protrusion elevated by ~0.68 Å from the adjacent (2 × 1) region on the same terrace.[11] Therefore, the formation of the (2 × 1) structure occurs via consuming the parent $c(6 \times 2)$ structure by $c(6 \times 2) \rightarrow (2 \times 1)$ transformation induced by the loss of the chemisorbed oxygen in the reacted region, which results in the co-existing (2 × 1) and c(6 × 2) domains on the same terrace. Fig. 1(c) also shows that all the (2 × 1) reconstructed regions are bordered with step edges, suggesting that the H_2 adsorption induced $c(6 \times 2) \rightarrow (2 \times 1)$ transformation is initiated from the step edge areas. In addition to its less surface coverage of oxygen, the (2 × 1) structure also has a smaller surface coverage of Cu atoms compared to the $c(6 \times 2)$ structure (the surface coverages of Cu atoms for the $c(6 \times 2)$ and (2 × 1) are θ = 5/6 and 1/2, which can be translated to the atomic surface densities of 0.07/Å^2 and 0.05/Å^2, respectively). Apparently, the formation of the (2 × 1) structure by consuming the existing $c(6 \times 2)$ requires the release of Cu atoms in addition to the loss of chemisorbed oxygen.

As seen from Fig. 1(c), Cu atoms released from the $c(6 \times 2) \rightarrow (2 \times 1)$ transformation aggregate and form clusters along step edges. As indicated by the arrows in Fig. 1(c), some Cu clusters also aggregate on the terrace in the (2 × 1) reconstructed regions. However, the parent $c(6 \times 2)$ reconstructed regions do not show any Cu clusters, clearly demonstrating that the formation of Cu clusters is related to the $c(6 \times 2) \rightarrow (2 \times 1)$ transformation (i.e., Cu clusters form only in the reacted region). STM imaging shows that Cu clustering happens preferentially on the upper side of step edges (e.g., Fig. 1(c)). This can be mainly attributed to the Ehrlich-Schwoebel (ES) barrier effect, which hinders Cu atoms from crossing descendent steps, thereby promoting 3D islanding. In addition, the preferential (6 × 2) → (2 × 1) transformation along the step edges also facilitates the clustering of Cu atoms in these regions. Meanwhile, the absence of Cu clusters in the $c(6 \times 2)$ regions (see Fig. 1(c)) suggests that the $c(6 \times 2)$ constructed surface does not serve as a favorable structure template for the clustering of Cu atoms. Instead, step edge regions are more defective (even with the presence of small bare Cu areas), which also contribute to the preferential formation of Cu clusters along step edges. In addition, the lack of Cu clusters on the c(6 × 2) region also suggests the existence of a significant kinetic hindrance for the migration of Cu atoms over the intact c(6 × 2) region. By contrast, the (2 × 1) reconstruction has a more open structure and Cu atoms released from the $c(6 \times 2)$/(2 × 1) boundary can diffuse in channels between Cu—O—Cu chains in the (2 × 1) regions.

Fig. 1(e) shows a typical STM image after the surface was further exposed to 5×10^{-5} Torr H_2 at 150 °C for ~16 h. Under such prolonged H_2 exposure at the higher pressure, the $c(6 \times 2)$ reconstructed surface is now completely transformed to the (2 × 1) structure, as exemplified by the zoom-in STM image shown in Fig. 1(f). Fig. 1(e) shows that Cu atoms released from the $c(6 \times 2) \rightarrow (2 \times 1)$ transformation now mostly aggregate along the step edge areas (e.g., the upper-left corner area) with scattered distribution of Cu clusters on the (2 × 1) reconstructed terrace. Some depressions are also seen to develop on the terrace, and depression regions have the row characteristic of the (2 × 1) restructuring.

B. DFT modeling of hydrogen adsorption and the associated atomic structure evolution

The STM experiments described above clearly show that the Cu(110)-$c(6 \times 2)$ reconstructed surface undergoes the transition to the (2 × 1) reconstruction upon the H_2 exposure. Yet, the atomic process leading to the $c(6 \times 2) \rightarrow (2 \times 1)$ is still not established due to the lack of the sufficient detectability in the STM imaging to resolve these details, including the nature of hydrogen adsorption, atom migration, and dynamics of the surface phase transition. We therefore employ DFT calculations to elucidate the atomic processes of the hydrogen adsorption induced surface structure evolution observed from the STM experiments.

Fig. 2 shows the surface structure of the relaxed Cu(110)-$c(6 \times 2)$ used as the starting surface for hydrogen adsorption. Because of the surface symmetry, there are only two nonequivalent on-top O sites, two nonequivalent on-top Cu sites, and five nonequivalent hollow sites. Five different kinds of the

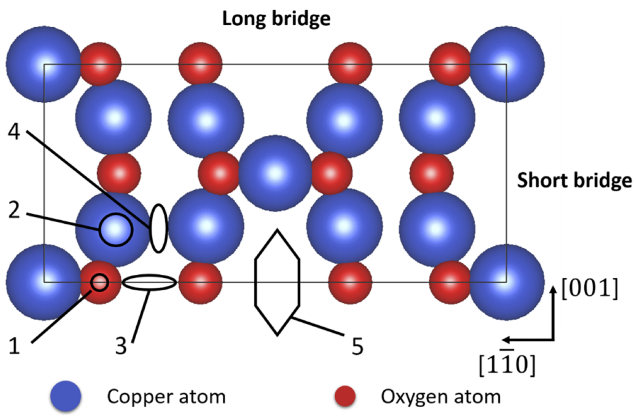

FIG. 2. Surface sites for the adsorption of H atoms or molecules on Cu(110)-c(6 × 2): (1) top of the O atom; (2) top of the Cu atom; (3) hollow between O atoms; (4) hollow between Cu atoms; (5) hexagonal hollow on the edge. The long-bridge and short-bridge directions are, respectively, along the [1$\bar{1}$0] and [001] directions of the cell edge.

adsorption sites at the Cu(110)-$c(6 \times 2)$ surface are investigated: top of O atoms, top of Cu atoms, hollow sites between neighboring O atoms, hollow sites between neighboring Cu atoms, and the hexagonal hollow sites along the edges of the unit cell. These different adsorption sites are numbered in Fig. 2. We consider the adsorption of both atomic and molecular hydrogen in order to determine the preferred type of the surface adsorption. For molecular adsorption, both the parallel and vertical configurations of H_2 adsorption are investigated. The parallel configuration includes two adsorption geometries of the H_2 molecule with its axis along the long bridge and short bridge directions of the $c(6 \times 2)$ cell, which correspond to the long and short edges the unit cell as shown in Fig. 2.

Our calculations of the adsorption energy for each case considered above show that hydrogen adsorbs preferentially at the top of O sites in the molecular form. Our results show that when a H_2 molecule horizontally approaches to the O site, it reacts with the O atom to form a water molecule that then desorbs from the surface without energy barriers. When the H_2 molecule approaches the surface in other geometries, such as vertically or in 45° angle to the surface, it will always be repelled into the vacuum above the surface. Additionally, the large dissociation energy (~4.5 eV[58]) of H_2 molecules suggests that the dissociative adsorption by the oxygenated Cu(110) surface is less favorable than the molecular adsorption (it should be noted that the barrier for dissociation of H_2 molecules on metallic Cu(111) is only 0.5 eV[6]). We employed NEB method to compute the energy barriers for the two processes: the horizontal approaching of a H_2 molecule onto an O site for H_2O formation and its desorption from the surface. At the beginning, one H_2 molecule is placed in the vacuum, ~1.25 Å above the top of the O atom (Fig. 3(a)), which is the initial image of the NEB calculation. Then, the H_2 molecule is placed horizontally in contact with the O atom (Fig. 3(b)) as the beginning image of the desorption calculation. In our adsorption calculations, the H_2 molecule placed on the O atom bonds with the O atom to form a H_2O molecule that spontaneously desorbs from the surface (Fig. 3(c)), which is also the final state in NEB calculation. The NEB energy plot (Fig. 3(d)) shows that this reaction has a barrier of ~2.68 eV when H_2 approaches the surface. The subsequent H_2O formation and desorption does not require any barriers, and the energy of the system drops significantly after the H_2O desorption. Cu sites are unfavorable sites for the adsorption of either atomic or molecular hydrogen (both show nearly zero adsorption energy). We also verified that the adsorption on hollow sites between Cu atoms or between O atoms is not favorable. Our calculations demonstrate that the hydrogen adsorption occurs on the top of chemisorbed O in the $c(6 \times 2)$ structure and produces H_2O molecules that desorb from the surface. The large adsorption barrier and the required horizontal adsorption configuration explain why the enormous amount of H_2 exposure is needed to transform the surface from the (6×2) reconstruction (O coverage = 2/3 ML) to the (2×1) reconstruction (O coverage = 0.5 ML) with the slight O loss. In our NEB calculations, the processes of H_2 approaching the surface and H_2O desorbing from the surface are treated separately, for which the detailed reaction sequence between H_2 molecule and a chemisorbed O cannot be revealed. However, our NEB results show that the H_2 molecule reacting with oxygen on the Cu surface is an activated process (Fig. 3), which can be related to the stretching of the H–H bond that costs energy and is a prerequisite for the H_2O formation reaction. The direct reaction of H_2 with a chemisorbed O to form a H_2O molecule shown here can be characterized as an Eley-Rideal surface reaction, in which a gas-phase reagent reacts directly with an adsorbed species and the reaction product either desorbs from or remains on the surface depending on the particular chemical reaction.[59]

The H adsorption induced loss of chemisorbed O in the $c(6 \times 2)$ reconstruction drives the $c(6 \times 2) \rightarrow (2 \times 1)$ transition. We then model the atomic process that leads to the surface phase transition. H adsorption reaction firstly removes one chemisorbed O atom from the $c(6 \times 2)$ cell to form a H_2O molecule that desorbs from the surface. Fig. 4(a) shows the starting $c(6 \times 2)$ structure and Fig. 4(b) shows the structure after the removal of the first O atom by the molecular H adsorption, where O-3 atom is the first one to be removed, as

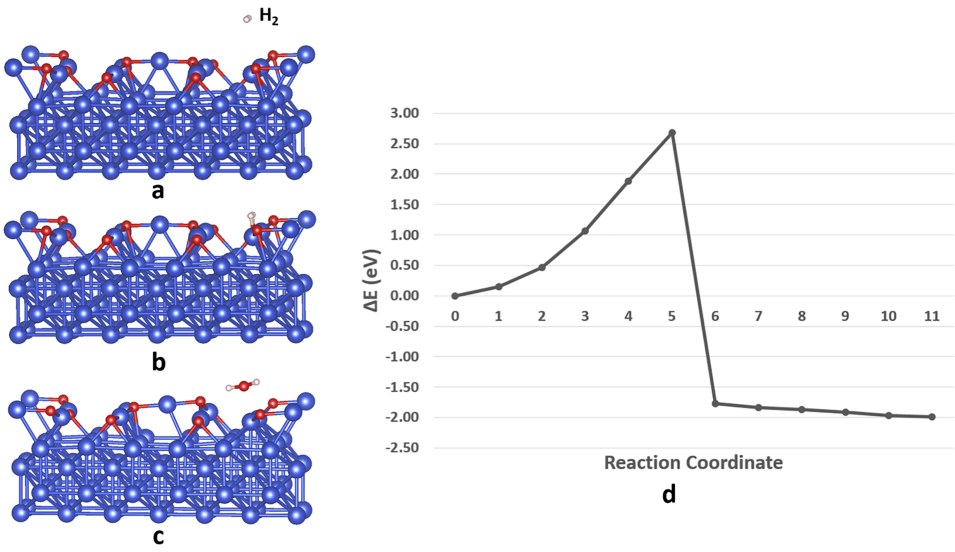

FIG. 3. (a) A H_2 molecule is placed in the vacuum above the Cu(110)-c(6 × 2) surface (i.e., image 0 shown in (d)); (b) the H_2 molecule just touches with the O atom at the surface (image 5 in (d)); (c) the relaxed structure of the horizontal H_2 adsorption, showing the formation of a H_2O molecule that desorbs from the surface (image 11 in (d)); (d) NEB energy plot of H_2 approaching to the Cu(110)-c(6 × 2) surface and the subsequent H_2O molecule desorption process. The H_2 molecule sits initially 1.25 Å above the top of the O atom and then moves 0.25 Å per image toward the O atom.

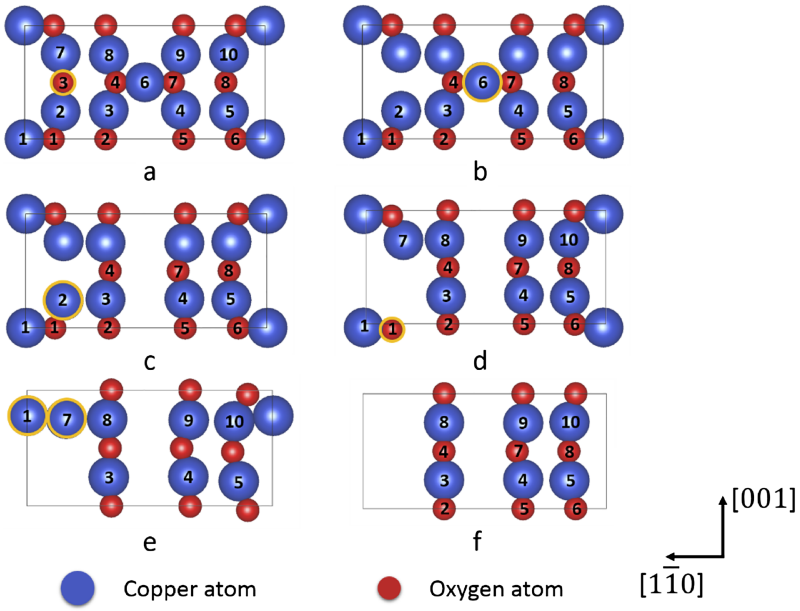

FIG. 4. Images of the unit cell in each step. (a) The $c(6 \times 2)$ structure; (b) the structure after removing first atom (O-3); (c) the structure after removing second atom (Cu-6); (d) the structure after removing third atom (Cu-2); (e) the structure after removing fourth atom (O-1); (f) the structure after removing the last two atoms (Cu-1 and Cu-7). Notations of O and Cu sites are defined in the figure. Atoms marked by yellow circles are removed sequentially from the cell.

identified from our hydrogen adsorption calculations described above. After the removal of the first O atom, the relaxed structure does not show appreciable difference from the parent $c(6 \times 2)$ structure. The stability of each top-surface atom was examined again after the loss of the first O atom. As already known from the calculations above, molecular H_2 adsorption on the O sites with the parallel configuration is much more favored than all the other cases; therefore, the adsorption of horizontally oriented H_2 molecules at the O atoms is examined in order to identify the subsequent O atoms that are most likely to leave from the surface by reacting with H_2 to form H_2O in later calculations. Because the unit cell has lost its symmetry along the [1$\bar{1}$0] direction after the removal of the first O atom, hydrogen adsorption energy should be examined at the seven remaining O atom sites, as indicated in Fig. 4(b).

The oxygen loss induced $c(6 \times 2) \rightarrow (2 \times 1)$ transition involves the ejection of Cu atoms from the parent $c(6 \times 2)$ structure (as shown in Fig. 1, these ejected Cu atoms aggregate to form Cu clusters). The strategy we used here is to calculate first the vacancy formation energy for Cu atoms. If it is close to zero, the respective Cu will diffuse away much faster than any activated reaction between H_2 and chemisorbed O that can occur. Only when all remaining Cu atoms in the unit cell are stable, then system will wait for the next reaction process that results in the loss of a chemisorbed O by reacting with a H_2 molecule. We therefore also examine the vacancy formation energy associated with the ejection of Cu atoms from the $c(6 \times 2)$ structure. Due to the mirror symmetry along the [001] direction, there are only 6 nonequivalent Cu atom sites that are required to examine, as numbered in Fig. 4(b). Table I lists the calculated energies for both the adsorption of hydrogen on O atoms and Cu vacancy formation at different surface sites. The results show that only Cu-6 has the negative vacancy formation energy, suggesting that this Cu atom can diffuse away easily, leaving a vacancy behind.

In addition, the total energy of the slab after removing the Cu atom is much lower than removing the O atom. Thus, the next atom to be removed ought to be the Cu atom at the Cu-6 site. After the loss of the first O atom, the unit cell becomes unstable and the Cu atom at the Cu-6 site can jump in the channel along the [001] direction because there are hollow sites available in the channel. Our NEB calculations show that the hopping of Cu-6 to its nearest hollow sites in the [001] channel requires overcoming an energy barrier of 0.85 eV, which is not significantly larger than that (~0.5 eV) for self-diffusion of Cu atoms on Cu(110).[24] Such in-channel diffusion with the modest energy barrier can be efficient for the elevated temperature (350 °C) of H_2 exposure. Fig. 4(c) illustrates the relaxed structure after removing the Cu atom at the Cu-6 site, which shows that the unit cell does not exhibit significant change because all the remaining atoms in the reconstructed layer are still connected well by Cu—O bonds. However, the Cu atom at the Cu-2 site is bonded by only one O atom, suggesting that the Cu atom is relatively unstable.

TABLE I. Energies for H_2 molecule adsorbed on remained O atoms and vacancy formation on Cu atom sites after removing the first atom. The relaxed structure is shown in Fig. 4(b). For O sites, suffix "S" means that the H_2 molecule is along the short bridge of $c(6 \times 2)$ cell and suffix "L" means that the H_2 molecule is along the long bridge of $c(6 \times 2)$ cell.

Site	E_{ads} (eV)	Site	E_{vac} (eV)
O-1-S	−0.05	Cu-1	0.18
O-1-L	0.27	Cu-2	0.12
O-2-S	−0.03	Cu-3	0.43
O-2-L	−1.01	Cu-4	0.27
O-4-S	−0.03	Cu-5	0.31
O-4-L	0.35	Cu-6	−0.10
O-5-S	−0.03		
O-5-L	−0.05		
O-6-S	−0.03		
O-6-L	−0.04		
O-7-S	−0.03		
O-7-L	−0.04		
O-8-S	−0.03		
O-8-L	−0.05		

TABLE II. Energies of H_2 molecule adsorption and vacancy formation on Cu atom sites after removing second atom from the unit cell. The relaxed structure is shown in Fig. 4(c).

Site	E_{ads} (eV)	Site	E_{vac} (eV)
O-1-S	–0.51	Cu-1	0.23
O-1-L	0.34	Cu-2	0.07
O-2-S	–0.03	Cu-3	0.44
O-2-L	–0.04	Cu-4	0.43
O-4-S	–0.03	Cu-5	0.38
O-4-L	–0.60		
O-5-S	–0.03		
O-5-L	–0.04		
O-6-S	–0.03		
O-6-L	–0.03		
O-7-S	–0.03		
O-7-L	–0.42		
O-8-S	–0.03		
O-8-L	–0.04		

TABLE III. Energies of H_2 molecule adsorption and vacancy formation on Cu atom sites after removing third atom from the unit cell. The relaxed structure is shown in Fig. 4(d).

Site	E_{ads} (eV)	Site	E_{vac} (eV)
O-1-S	–0.70	Cu-1	0.26
O-1-L	0.33	Cu-3	0.33
O-2-S	–0.04	Cu-4	0.44
O-2-L	–0.04	Cu-5	0.44
O-4-S	–0.04	Cu-7	0.34
O-4-L	–0.04	Cu-8	0.41
O-5-S	–0.04	Cu-9	0.46
O-5-L	–0.04	Cu-10	0.42
O-6-S	–0.04		
O-6-L	0.57		
O-7-S	–0.04		
O-7-L	–0.44		
O-8-S	–0.04		
O-8-L	–0.04		

To find the third atom to be removed from the remaining cell, we perform the same test as in the previous steps. Table II shows that the vacancy formation energy for the Cu atom at the Cu-2 site nearly equals to zero. This indicates that the Cu atom at the Cu-2 site is likely to be the next atom to leave from the unit cell. Fig. 3(d) shows the relaxed structure of the unit cell after the ejection of the Cu atom at the Cu-2 site. Comparing the two relaxed structures before and after removing the third atom from the unit cell, we can find that the Cu atoms at the Cu-1 and Cu-7 sites and the O atom at the O-1 site move down slightly because of the loss of the Cu atom at the Cu-2 site (note that the Cu and O atoms at the lower-left corners are equivalent to the atoms at the upper-left corners; therefore the Cu atoms at the Cu-1 and Cu-7 sites and the O atom at the O-1 site form a Cu—O—Cu chain). To continue this process, we calculate the adsorption energy and vacancy formation energy of Cu again and identify the next atom to be removed from the cell. As shown in Fig. 4(d), the structure of the unit cell has lost its symmetry in both [001] and $[1\bar{1}0]$ directions, and thus the adsorption of H on all O atoms as well as the stability of all Cu atoms in the unit cell are required to be examined. The results of calculated energies are listed in Table III, which show that no Cu atom site has very low vacancy formation energy, suggesting that the ejection of any Cu atom is not favored in this step. Instead, the O atom at the O-1 site has extremely low adsorption energy, indicating the ejection of this O atom by reacting with H_2 molecule is very likely.

Fig. 4(e) shows the relaxed structure after the removal of the four atoms shown above. It can be seen from Fig. 4(e) that the Cu atom at the Cu-7 site has lost all its neighboring O atoms, which can be considered now as a free Cu atom at the surface. The Cu atom at the Cu-1 site has also lost its Cu–O bonds (note that the Cu atom on the right-hand side of the Cu atom at the Cu-10 site is equivalent to the Cu atom at the Cu-1 site). Therefore, the two Cu atoms at the Cu-1 and Cu-7 sites tend to be unstable. To verify this assumption, the stability of the two Cu sites is examined and the results are listed in Table IV. Both the Cu-1 and Cu-7 sites have nearly zero vacancy formation energy, confirming that these two Cu atoms can easily diffuse away from the unit cell. Based on the stability results, these two unstable Cu atoms are thus removed in the last step, Fig. 4(f) shows the relaxed structure after removing these two Cu atoms.

The resulting structure obtained in this step is very similar to the (2 × 1) configuration (Fig. 4(f)), except for the smaller spacing between the Cu—O—Cu chains in the middle and on the right hand side. The displacement of the rightmost Cu—O—Cu chain by another $[1\bar{1}0]$-(1 × 1) lattice spacing toward the right-hand side would result in the formation of the (2 × 1) configuration. The unit cell now contains three Cu—O—Cu chains, the Cu and O atoms in the Cu—O—Cu chains in the middle and on the right hand side show slight zigzag configuration along the [001] chain direction. The misalignment of the Cu and O atoms in these two chains suggests that these atoms have the tendency to reorganize and form a more stable configuration.

After removing the two O atoms and four Cu atoms from the unit cell, the configuration shown in Fig. 4(f) requires now few diffusion processes of selected atoms within the unit cell to become the final (2 × 1) structure. To model this diffusion process, we normally should start from identifying the most unstable atom in the Cu—O—Cu chain on the right, then moving it further toward to the right side by an $[1\bar{1}0]$-(1 × 1)

TABLE IV. Energies of vacancy formation on Cu atom sites after removing fourth atom from the unit cell. The relaxed structure is shown in Fig. 4(e).

Site	E_{vac} (eV)
Cu-1	–0.10
Cu-3	0.26
Cu-4	0.41
Cu-5	0.27
Cu-7	0.01
Cu-8	0.36
Cu-9	0.48
Cu-10	0.26
Cu-1 and Cu-7	–0.47

lattice spacing, and then following the similar step by moving the second unstable atoms. However, our NEB calculation results show that such an atom-by-atom migration process is kinetically unfavorable at the typical temperature because the energy barrier is higher than 1.00 eV. An alternative scenario is that the Cu—O—Cu chain on the right side can move toward the right edge of the unit cell as whole without breaking Cu–O bonds. If the whole chain can move together to its final position with only a small energy barrier, it can prove that the second pathway is more favored.

Fig. 5(a) shows the NEB calculation result of the energy barrier for the migration of the whole Cu—O—Cu chain, which is 0.33 eV, much smaller than the pathway via the migration of individual Cu and O atoms that requires the breaking of Cu–O bonds. Additionally, this diffusion process of the Cu—O—Cu chain results in the drop of the system energy by 0.40 eV. Figs. 5(c)–5(g) show the configurations of the intermediate diffusion steps obtained from NEB starting with the structure shown in Fig. 5(b), which is the same configuration as in Fig. 4(f). Fig. 5(h) shows the final structure of the last diffusion step, which has the (2 × 1) configuration. As shown in Fig. 5(b), the Cu—O—Cu chain on the right initially shows slight bending toward the left, and O atoms at the two ends (i.e., located at the upper and lower edges of the unit cell) have stronger tendency of moving toward the right than the O atom in the middle of the Cu—O—Cu chain. Therefore, the Cu—O—Cu chain migration is initiated by these two O atoms at the cell edge, which pull the neighboring Cu atoms toward the right side and then the O atom in the middle to the right side in the [$\bar{1}$10] direction. After moving one [$\bar{1}$10]-(1 × 1) lattice spacing, the whole chain reaches the right edge of the unit cell and all atoms occupy the stable sites. The structure is now the same as the (2 × 1) configuration. The size of the unit cell used in our calculations may be too small to provide a comprehensive picture of the diffusion process. In reality, the diffusion of a long chain as a whole is practically impossible. Instead, the diffusion of small Cu–O clusters such as dimers and trimers is more feasible. This trend can be discerned from Fig. 4, which shows that the atoms at the cell edges move faster than the atoms in the middle. Provided that a large cell is used in the simulation, the curvature of the migrating chain is likely to become larger, which tends to break the chain into smaller segments.

The Cu—O—Cu chain migration shown in the simulation (Fig. 5) has also been observed from our STM experiment. Fig. 6 illustrates time-sequence STM images of the Cu(110) surface showing the migration of Cu—O—Cu chains. Fig. 6(a) shows a (2 × 1) island and a single Cu—O—Cu chain (labeled as A) with a lateral distance of 1.5 nm from the island. As seen in Fig. 6(b), the top segment of Cu—O—Cu chain A shifts toward the left by ~0.5 nm, resulting in a larger spacing (2 nm) between the shifted segment and the (2 × 1) island. Meanwhile, another Cu—O—Cu chain (labeled as B) grows from the bottom-right corner into the field of view. The chain migration is further revealed from Fig. 6(c), which shows that the bottom-right segment of chain A shifts laterally in the [$\bar{1}$10] direction and chain B also shifts laterally in the same direction and by the same amount. Therefore, chains A and B now become a single chain by such coordinated shifting of the two segments. It can be also noted from Fig. 6(c) that the top segment of chain A shifts laterally toward the [$\bar{1}$10] direction, resulting in a smaller spacing (1 nm) with the (2 × 1) island. Fig. 6(d)

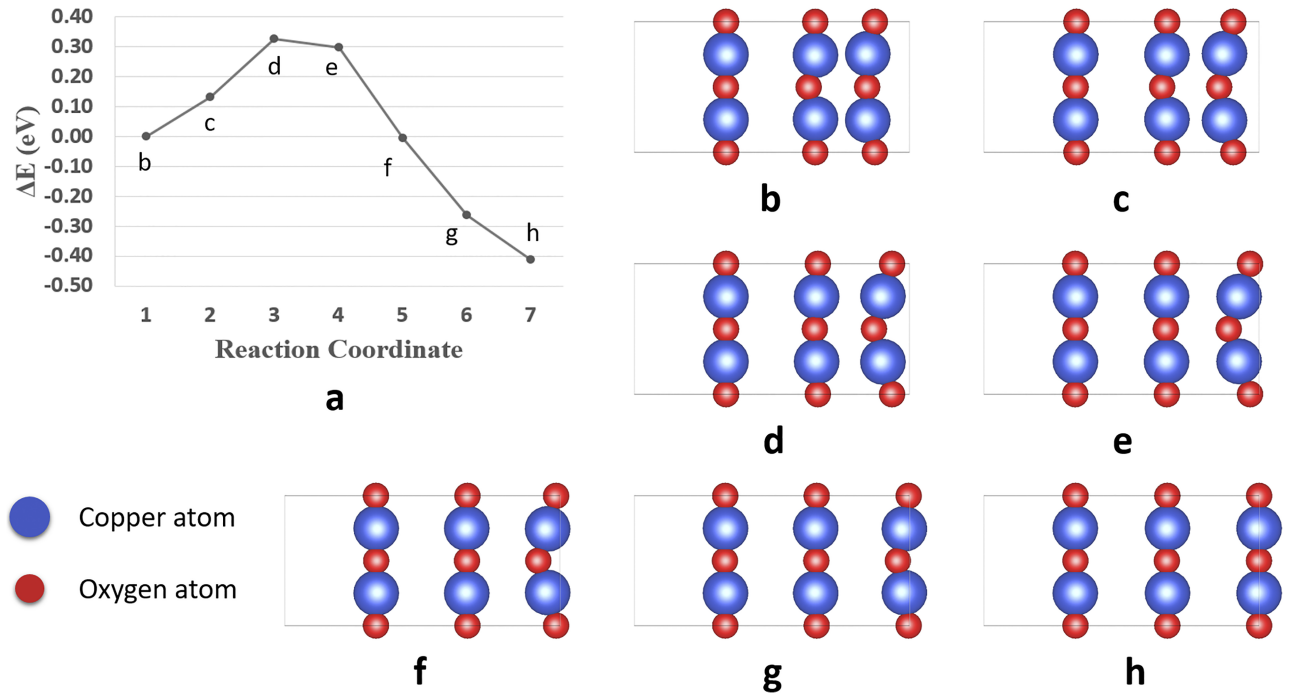

FIG. 5. (a) NEB energy plot for the chain diffusion process of the rightmost Cu—O—Cu chain shown in the starting structure (b) and (c)–(g) the relaxed intermediate structures of NEB images; (h) the final image of the NEB calculation, which shows the arrival of the (2 × 1) configuration after the migration of the Cu—O—Cu chain by one [1$\bar{1}$0]-(1 × 1) lattice spacing toward the right-hand side.

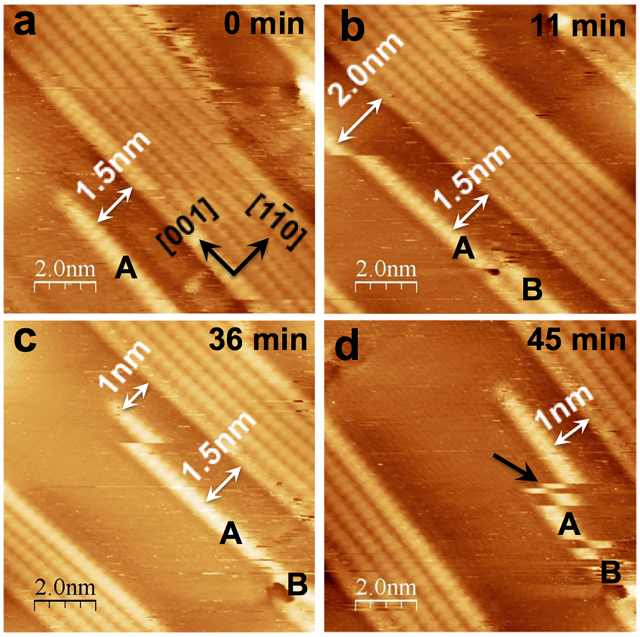

FIG. 6. Time-sequence STM images showing the migration of Cu—O—Cu segments during the exposure of the Cu(110) to 1×10^{-10} Torr O_2 at room temperature. The tunneling conditions for the STM imaging are $I_T = 0.1$ nA and $V_B = -1.4$ V.

shows that the shifted segment becomes longer because of the lateral shifting of more Cu—O—Cu species in chain A toward the (2×1) island. A moving STM tip can induce motion of atoms or atom clusters on a surface, which often shows dramatic movements or accompanies imperfect feature images. In Fig. 6(d), the zigzag appearance of some Cu—O—Cu segments (indicated by the black arrow in Fig. 6(d)) can be induced either by the moving STM tip or the highly mobile nature of the Cu—O—Cu segments, which cannot be readily distinguished from a single scan. Because we monitored the chain migration in sequential scannings, the motion induced by diffusion can show some characteristic feature in sequential images, which differs from the abrupt feature induced by an STM tip. If the lateral movement of the Cu—O—Cu chains is a thermally activated process, one would expect a random walk as long as the surface diffusion potential is not affected by the neighboring (2×1) island. The latter, however, should be negligible for a distance of 1.5 nm. The top segment of chain A shifts first toward the left by ~ 0.5 nm (Fig. 6(b)), then shifts toward the right by ~1 nm (Figs. 6(c) and 6(d)). This indicates that the direction for the side-way movement is random, suggesting that the chain motion is thermally induced by the chain diffusion rather than the tip induced artifact.

IV. CONCLUSIONS

The results presented here provide atomic level insight into the hydrogen adsorption induced Cu(110)-$c(6 \times 2)$-O $\rightarrow (2 \times 1)$ transition induced by the loss of chemisorbed oxygen. It is shown that hydrogen adsorption takes place horizontally in its molecular form on top of chemisorbed oxygen, which results in the formation of H_2O molecules that desorb spontaneously from the surface. Using DFT and NEB calculations, we further identify the reaction pathway for the $c(6 \times 2) \rightarrow (2 \times 1)$ transition, which matches with the STM observations. This work has brought new insight into the reaction mechanism of chemisorbed oxygen with ambient hydrogen including adsorption, diffusion, and reorganization of the surface structure, which can have practical importance because the lively surface dynamics induced by the gas-surface reactions will affect the surface chemical properties under realistic conditions, and, for instance, catalytic reactions taking place over oxygenated surfaces.

ACKNOWLEDGMENTS

This work was supported by the National Science Foundation under NSF CAREER Award Grant No. CMMI-1056611 and NSF Collaborative Research Award Grant No. CBET-1264940. W. Saidi acknowledges the support of NSF under Grant No. DMR-1410055. The authors thank N. P. Guisinger for help with the STM experiments. Research carried out in part at the Center for Nanoscale Materials, Argonne National Laboratory, which is supported by the U.S. Department of Energy, Office of Basic Energy Sciences, under Contract No. DE-AC02-06CH11357 and at the Center for Functional Nanomaterials, Brookhaven National Laboratory, which is supported by the U.S. Department of Energy, Office of Basic Energy Sciences, under Contract No. DE-AC02-98CH10886. This work used the computational resources from the Extreme Science and Engineering Discovery Environment (XSEDE), which is supported by National Science Foundation Grant No. OCI-1053575.

[1] T. Punniyamurthy and L. Rout, Coord. Chem. Rev. **252**(1-2), 134–154 (2008).
[2] L. Österlund, P. Rasmussen, P. Thostrup, E. Lægsgaard, I. Stensgaard, and F. Besenbacher, Phys. Rev. Lett. **86**(3), 460 (2001).
[3] L. H. Germer and A. U. MacRae, J. Chem. Phys. **37**(7), 1382 (1962).
[4] D. E. Ibbotson, T. S. Wittrig, and W. H. Weinberg, J. Chem. Phys. **72**(9), 4885 (1980).
[5] J. R. Engstrom, W. Tsai, and W. H. Weinberg, J. Chem. Phys. **87**(5), 3104 (1987).
[6] B. Hammer, M. Scheffler, K. W. Jacobsen, and J. K. Nørskov, Phys. Rev. Lett. **73**(10), 1400 (1994).
[7] T. R. Mattsson, G. Wahnström, L. Bengtsson, and B. Hammer, Phys. Rev. B **56**(4), 2258 (1997).
[8] G. Kresse, Phys. Rev. B **62**(12), 8295 (2000).
[9] G. Kresse and J. Hafner, Surf. Sci. **459**(3), 287–302 (2000).
[10] K. Christmann, Prog. Surf. Sci. **48**(1), 15–26 (1995).
[11] Q. Liu, L. Li, N. Cai, W. A. Saidi, and G. Zhou, Surf. Sci. **627**, 75–84 (2014).
[12] F. Besenbacher and J. K. Nørskov, Prog. Surf. Sci. **44**(1), 5–66 (1993).
[13] D. Coulman, J. Wintterlin, J. Barth, G. Ertl, and R. Behm, Surf. Sci. **240**(1), 151–162 (1990).
[14] D. Coulman, J. Wintterlin, R. Behm, and G. Ertl, Phys. Rev. Lett. **64**(15), 1761 (1990).
[15] R. Feidenhans, F. Grey, M. Nielsen, F. Besenbacher, F. Jensen, E. Lægsgaard, I. Stensgaard, K. W. Jacobsen, J. K. Nørskov, and R. Johnson, Phys. Rev. Lett. **65**(16), 2027 (1990).
[16] L. Sun, M. Hohage, and P. Zeppenfeld, Phys. Rev. B **69**(4), 045407 (2004).
[17] L. Sun, M. Hohage, R. Denk, and P. Zeppenfeld, Phys. Rev. B **76**(24), 245412 (2007).
[18] L. Guillemot and K. Bobrov, Phys. Rev. B **83**(7), 075409 (2011).
[19] L. Li, Q. Liu, J. Li, W. A. Saidi, and G. Zhou, J. Phys. Chem. C **118**(36), 20858–20866 (2014).
[20] F. Jensen, F. Besenbacher, E. Lægsgaard, and I. Stensgaard, Phys. Rev. B **42**(14), 9206 (1990).
[21] F. Jensen, F. Besenbacher, E. Lægsgaard, and I. Stensgaard, Phys. Rev. B **41**(14), 10233 (1990).
[22] K. Kern, H. Niehus, A. Schatz, P. Zeppenfeld, J. Goerge, and G. Comsa, Phys. Rev. Lett. **67**(7), 855 (1991).

[23]F. Frechard and R. Van Santen, Surf. Sci. **407**(1), 200–211 (1998).
[24]S. Liem, J. Clarke, and G. Kresse, Surf. Sci. **459**(1), 104–114 (2000).
[25]S. Liem, G. Kresse, and J. Clarke, Surf. Sci. **415**(1), 194–211 (1998).
[26]X. Duan, O. Warschkow, A. Soon, B. Delley, and C. Stampfl, Phys. Rev. B **81**(7), 075430 (2010).
[27]G. Zhou, L. Luo, L. Li, J. Ciston, E. A. Stach, and J. C. Yang, Phys. Rev. Lett. **109**(23), 235502 (2012).
[28]I. Wachs and R. Madix, J. Catal. **53**, 208 (1978).
[29]I. E. Wachs and R. J. Madix, Surf. Sci. **76**(2), 531–558 (1978).
[30]S. Sakong and A. Gross, J. Phys. Chem. A **111**(36), 8814–8822 (2007).
[31]M. K. Bradley, D. K. Lorenzo, W. Unterberger, D. A. Duncan, T. Lerotholi, J. Robinson, and D. Woodruff, Phys. Rev. Lett. **105**(8), 086101 (2010).
[32]P. Singnurkar, I. Bako, H. Koch, E. Demirci, A. Winkler, and R. Schennach, J. Phys. Chem. C **112**(36), 14034–14040 (2008).
[33]J. Li and G. Zhou, Surf. Sci. **646**, 288–297 (2016).
[34]P. Hohenberg and W. Kohn, Phys. Rev. **136**(3B), B864–B871 (1964).
[35]W. Kohn and L. J. Sham, Phys. Rev. **140**(4A), A1133–A1138 (1965).
[36]R. G. Parr and W. Yang, *Density-Functional Theory of Atoms and Molecules* (Oxford University Press, 1989).
[37]R. M. Martin, *Electronic Structure: Basic Theory and Practical Methods* (Cambridge University Press, 2004).
[38]R. M. Dreizler and E. K. Gross, *Density Functional Theory: An Approach to the Quantum Many-Body Problem* (Springer Science & Business Media, 2012).
[39]G. Kresse and J. Furthmüller, Phys. Rev. B **54**(16), 11169 (1996).
[40]G. Kresse and J. Furthmüller, Comput. Mater. Sci. **6**(1), 15–50 (1996).
[41]G. Kresse and J. Hafner, Phys. Rev. B **49**(20), 14251 (1994).
[42]G. Kresse and D. Joubert, Phys. Rev. B **59**(3), 1758 (1999).
[43]J. P. Perdew, J. Chevary, S. Vosko, K. A. Jackson, M. R. Pederson, D. Singh, and C. Fiolhais, Phys. Rev. B **46**(11), 6671 (1992).
[44]P. E. Blöchl, Phys. Rev. B **50**(24), 17953 (1994).
[45]G. Zhou, L. Luo, L. Li, J. Ciston, E. A. Stach, W. A. Saidi, and J. C. Yang, Chem. Commun. **49**(92), 10862–10864 (2013).
[46]L. Li, N. Cai, W. A. Saidi, and G. Zhou, Chem. Phys. Lett. **613**, 64–69 (2014).
[47]L. Li, L. Luo, J. Ciston, W. A. Saidi, E. A. Stach, J. C. Yang, and G. Zhou, Phys. Rev. Lett. **113**(13), 136104 (2014).
[48]W. A. Saidi, M. Lee, L. Li, G. Zhou, and A. J. H. McGaughey, Phys. Rev. B **86**(24), 245429 (2012).
[49]H. J. Monkhorst and J. D. Pack, Phys. Rev. B **13**(12), 5188 (1976).
[50]A. Tkatchenko and M. Scheffler, Phys. Rev. Lett. **102**(7), 073005 (2009).
[51]W. Al-Saidi, V. K. Voora, and K. D. Jordan, J. Chem. Theory Comput. **8**(4), 1503–1513 (2012).
[52]D. C. Sorescu, J. Lee, W. A. Al-Saidi, and K. D. Jordan, J. Chem. Phys. **134**(10), 104707 (2011).
[53]W. Al-Saidi, H. Feng, and K. A. Fichthorn, Nano Lett. **12**(2), 997–1001 (2012).
[54]W. A. Saidi, H. Feng, and K. A. Fichthorn, J. Phys. Chem. C **117**(2), 1163–1171 (2013).
[55]H. Jónsson, G. Mills, and K. W. Jacobsen, Classical Quantum Dyn. Condens. Phase Simul. **1**, 385–404 (1998).
[56]K. Momma and F. Izumi, J. Appl. Crystallogr. **44**(6), 1272–1276 (2011).
[57]P. Cabrera-Sanfelix, C. Lin, A. Arnau, and D. Sanchez-Portal, J. Phys.: Condens. Matter **25**(13), 135003 (2013).
[58]K. Piszczatowski, G. Łach, M. Przybytek, J. Komasa, K. Pachucki, and B. Jeziorski, J. Chem. Theory Comput. **5**(11), 3039–3048 (2009).
[59]W. H. Weinberg, Acc. Chem. Res. **29**(10), 479–487 (1996).